Optics & Laser Technology 54 (2013) 141–147

Contents lists available at ScienceDirect

Optics & Laser Technology

journal homepage: www.elsevier.com/locate/optlastec

Stochastic method for determining the coherence length of a TEA CO_2 laser

J. Codnia [a], N.D. Gómez [a], M.L. Azcárate [a,b,*]

[a] Departamento de Investigaciones en Láseres y Aplicaciones DEILAP (CITEDEF), Juan Bautista de La Salle 4397, B1603ALO Buenos Aires, Argentina
[b] Carrera del investigador, CONICET, Argentina

ARTICLE INFO

Article history:
Received 27 December 2012
Received in revised form
25 April 2013
Accepted 20 May 2013
Available online 14 June 2013

Keywords:
TEA CO_2 laser
Coherence length
Emission spectrum

ABSTRACT

In this work the results of the measurement of the coherence length of a TEA CO_2 laser developed in DEILAP are presented. A Michelson interferometer of about 5 m of optical path length difference was built for this purpose. A motorized translation optical mount was placed in one arm in order to enable the variation of the optical path length in many wavelengths. The length of the other arm was varied manually in steps of several tens of centimeters. Spatial filtering forced the laser to oscillate in a single transverse mode, TEM_{00}. An innovative stochastic technique for data analysis allowed determining the amount of longitudinal modes, the amplitude and the individual average coherence length of each mode as well as the global coherence length of the laser. This technique was later compared with a method based on the analysis of the Fourier transform of the time series obtained at the interferometer input.

1. Introduction

TEA CO_2 lasers have become essential tools for laser chemistry studies and for optical pumping of far-infrared (FIR) lasers due to their high efficiency, high power and wide tuning range. Infrared multiple photon dissociation (IRMPD) with TEA CO_2 lasers has been extensively used to induce chemical reactions of molecules in the ground electronic state [1–4], to study energy transfer processes in molecules [5,6], to generate radicals for specific kinetic studies [7–10] and as an isotope separation technique [2,3,11–13].

In all these applications the main requirement is the coincidence of the molecular absorption bands with a laser emission line. TEA CO_2 lasers usually work in multimode regimes (transverse and longitudinal) having broad linewidths or large beam quality factors, M^2, [14]. The presence of transverse modes is due to the fact that the characteristic transverse size of the gain medium is larger than the equivalent diameter of the TEM_{00} mode given by the resonator geometry. On the other hand, the longitudinal modes result from the resonator length and the gain spectral width of the active medium.

The large homogeneous linewidth of TEA CO_2 lasers enhance the possibility of the abovementioned matches. Nevertheless, low pumping efficiencies of molecular gas lasers are often attained with TEA CO_2 lasers due to the linewidth mismatch between the pump laser emission line and the absorption lines in the laser gas [15–17]. Likewise, IRMPD is based on the sequential absorption of photons resonant with a rovibrational mode of the molecule. In many cases of interest, the molecular absorption bands of different molecules or isotopomers are very close or even partly overlap making selective excitation difficult despite the laser tuning capability [2,3]. These drawbacks can be overcome by narrowing the linewidth of the TEA CO_2 laser. Different techniques have been reported for this purpose [15–20].

Since the excitation selectivity will strongly depend on the laser emission spectral width, it is of great interest to measure it. The spectral width is closely related to the emission source coherence. Highly monochromatic sources have large coherence lengths. The emission linewidth can be determined with both spectrometric and interferometric techniques. Optical spectrum analyzers based on Fabry–Perot interferometers with instrumental functions of ~10^{-2} cm^{-1} (~300 MHz) have been usually used to measure the linewidths of pulsed IR lasers [21]. A technique based on the double IR–IR resonance absorption using tunable diode lasers was later implemented to measure the spectral linewidth of a TEA CO_2 laser with higher spectral resolution of ~10^{-3} cm^{-1} (~30 MHz) [22]. Very accurate spectrum analyzers based on Michelson interferometers, Fizeau interferometers or on a combination of Fabry–Perot interferometers are now commercially available. These high resolution instruments used for coherence length measurements are quite expensive. The highest accuracy can be attained with Michelson, Sigmameter, Fabry–Perot and Fizeau wavemeters [23].

* Corresponding author at: Departamento de Investigaciones en Láseres y Aplicaciones DEILAP (CITEDEF), Juan Bautista de La Salle 4397, B1603ALO Buenos Aires, Argentina. Tel.: +54 1147098201.
E-mail addresses: jcodnia@citedef.gob.ar (J. Codnia), ndgomez@citedef.gob.ar (N.D. Gómez), lazcarate@citedef.gob.ar (M.L. Azcárate).

0030-3992/$ - see front matter © 2013 Elsevier Ltd. All rights reserved.
http://dx.doi.org/10.1016/j.optlastec.2013.05.025

In this work a technique for measuring the coherence length of a TEA CO_2 laser based on a Michelson interferometer is described. A Michelson interferometer was built for this purpose and the dependence of the variation of the intensity contrast of the interference fringes on the optical path length difference of both beams was measured. The optical path length was varied in discrete steps from some centimeters to about 5 m in one arm and, in the other, several millimeters around a fixed position. Due to the low reproducibility of the interference fringes pattern produced by pulse-to-pulse variations of the beam pointing stability, a novel method of stochastic analysis was developed for determining this contrast parameter. The coherence length of the laser was determined from the measurement of the variation of this parameter with the proposed method. The spectral linewidth of the laser was then derived. This technique was later compared with a method based on the Fourier transform analysis of the time series obtained at the interferometer input.

2. Materials and methods

The experimental setup scheme implemented is shown in Fig. 1.

A homemade TEA CO_2 laser was used as emission source. The laser resonator consisted of a rear plane mirror, M1, 100% reflectivity, and a Ge output coupler, M2, 60% reflectivity and 5 m focal length separated by a distance $L=135$ cm. The laser lased on the largest gain line, 10P(20) ($\lambda=10.6$ μm), with an output energy of 4 J at a repetition rate of 1 Hz. An intracavity iris, i, was placed near the plane mirror so as to modify through spatial filtering the amount of transverse modes of the emission. The iris diameter was set at $d=7$ mm in order to coincide with the diameter calculated from the output coupler focal distance and the cavity length for the TEM_{00} mode [14]. A concave mirror, M3, 2 m focal length, was used to collimate and introduce the laser beam into the Michelson interferometer consisting of two mirrors, M4 and M5, and a beam splitter, BS2. The optical path length difference in the interferometer was $z=2(L_1-L_2)$, with L_1 and L_2, the lengths of each arm. The optical path length of one beam, L_1, could be varied between 18 cm and 235 cm by the displacement of mirror M4. The optical path length of the other beam, L_2, was defined by moving mirror M5, placed on a motorized translation optical mount, Newport Motion Controller 860-C2, a total distance of about 1 cm around a fixed length of 18 cm at 70 μm/s. These values of L_1 and L_2 resulted in a variation range of z between 1 cm and 435 cm. Two homemade Ge semiconductor Photon Drag detectors (D1 and D2) were used to measure the laser intensity. Their response times of 0.4–1 ns allowed to achieve optical spectral resolutions larger than 1 GHz. A 1 mm pinhole was placed in front of detector D2 so as to detect only a small portion of the interference fringes pattern and, therefore, improve the contrast. The laser output energy was monitored with detector D1 from the beam reflection on a beamsplitter, BS1. The signals obtained with both detectors were digitized with an oscilloscope Tektronix DPO 7054, 500 MHz, 10 GS/s.

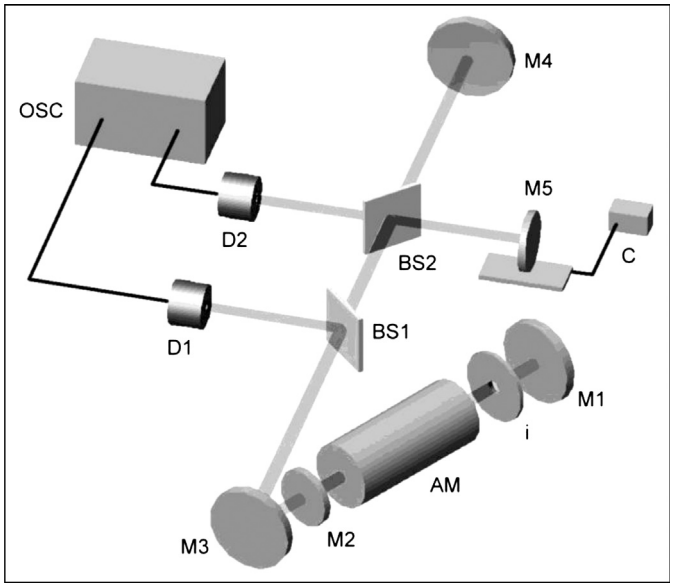

Fig. 1. Experimental setup. M1: 100% reflectivity laser mirror; M2: laser output coupler; AM: laser active medium; i: intracavity iris; M3: collimating mirror; BS1 and BS2: beam splitters; M4 and M5: interferometer's mirrors; C: motorized translation optical mount driver; D1 and D2: Photon Drag detectors; and OSC: oscilloscope.

As mentioned before there was a lack of reproducibility of the interference fringes pattern produced mainly by slight pulse-to-pulse angular variations of the beam. The spacing between the interference fringes maxima corresponds to half wavelength, 5 μm in this case. On the other hand, the beam round trip from the rear laser mirror M1 to the detector D2 was near 10 m and the interference fringes spacing was about 5 mm. Therefore, angular variations smaller than 1 mrad are comparable to displacements of about $\lambda/2$ of the motorized arm. This led to perform the sweep of one of the interferometer's arms with the motorized translation unit in an uncorrelated manner with the acquisition system. The measurement method was as follows: for each of the 13 positions of the mirror M4, 1000 time series were acquired at 1 Hz, sweeping the position of mirror M5 at 70 μm/s. Fig. 2 shows a typical time series characterized by a 60 ns spike (FWHM) followed by a ~2 μs tail. The observable of interest was the maximum value of this time series defined as the signal peak value (6.4 mV in Fig. 2).

Two series of 1000 signal peak values each are shown in Fig. 3 for two values of the optical path difference. It can be seen that for $z=1.1$ cm the pulse-to-pulse fluctuation of the signal peak value is much larger than for $z=86.5$ cm. In order to check the interferometer balance, 25 time series of the intensity of each arm were acquired both at the beginning and at the end of each series of 1000 measurements (in Fig. 3 values between 1 and 50 and between 1050 and 1100, respectively).

3. Calculations

For a given optical path difference z, the signal detected at the interferometer output can be described as the mean time value of the laser radiation intensity:

$$I(z) = I_0 \int_{-\infty}^{\infty} dk\, \Gamma(k)\Gamma^*(k)(1 + \cos(kz)) \tag{1}$$

where I_0 is the laser intensity at the interferometer input and $\Gamma(k)$, its emission spectrum. Lasing in single transverse mode (M^2~1) is achieved by space filtering with the intracavity iris. However, since there are still several longitudinal modes in the gain curve, the emission spectrum $\Gamma(k)$ can be modeled as a discrete sum of Lorentz functions of spectral width $\Delta\nu=c\gamma$ and amplitude b_n, centered in the wave numbers $k_n=k_0+n\pi/L$, where L is the laser resonator length. Under this assumption, expression (1) results

$$I(z) = I_0(1 + a(z)\cos(k_0 z)) \tag{2}$$

where k_0 is the wave number of the emitted radiation and $a(z)$, the interference fringes pattern contrast parameter defined as

$$a(z) = e^{-\gamma z}\frac{1 + 2\sum_{n=1}^{N} b_n \cos(n(\pi/L)z)}{1 + 2\sum_{n=1}^{N} b_n} \tag{3}$$

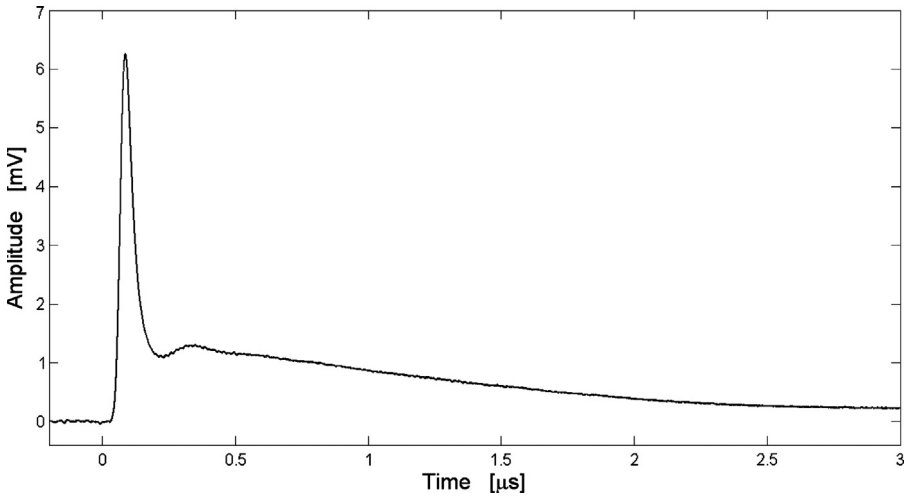

Fig. 2. Typical time series obtained with the Photon Drag detector, D2.

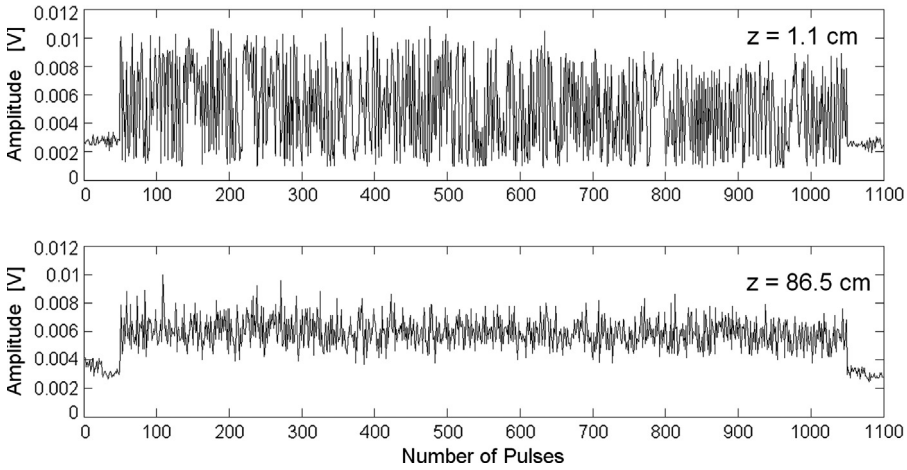

Fig. 3. Signal peak values registered for two series of 1000 measurements each of the optical path difference.

Expression (3) shows that the global coherence length, *Cl*, depends on the coherence length of each individual mode, γ^{-1}, and on the mode beating with their weight factors b_n.

Two clearly different length scales can be distinguished from expression (2): one, with a fast variation of about 5 μm ($\lambda/2$) given by the argument of the cosine function and, the other, with a slow variation of several tens of centimeters given by the variation of the contrast parameter.

The motorized translation unit swept small distances in an uncorrelated manner with the laser pulses allowing, thus, to determine $a(z)$ from the low frequency envelope value.

The weight factors b_n can be derived from the experimental values of $a(z)$ determined for diverse optical path differences. These factors indicate the number of oscillating modes and their relative amplitudes. Additionally, the coherence length of a single mode, γ^{-1}, is obtained.

Two random variables x and y were considered for the model described by expression (2). One was related to the laser intensity, I_0, normalized to its mean value

$$x = \frac{I_0}{\tilde{I}_0} \tag{4}$$

and the other,

$$y(z) = 1 + a(z)\cos(k_0 z) \tag{5}$$

was associated to the phase angle $k_0 z$. A Gaussian probability density function, pdf, with mean value 1 and standard deviation σ was chosen for x. Since there is no correlation between the sweep speed of the motorized translation unit and the laser repetition rate, a uniform pdf with values between 0 and 2π was chosen for the phase $k_0 z$. When the cosine function is applied to a phase uniform distribution, the probability of obtaining values close to zero decreases while that of obtaining values near –1 and 1 greatly increases. Since the contrast parameter $a(z)$ is not a random variable, a distribution varying between $1-a(z)$ and $1+a(z)$ results from expression (5). Therefore, the experimental values obtained will be described by a pdf, $h(I)$, derived from the product $I=xy$ of two random variables:

$$h(I) = \int_{-\infty}^{\infty} dx\, \frac{g(x)}{|x|} f\left(y = \frac{I}{x}\right) \tag{6}$$

with

$$g(x) = \frac{e^{-(x-1)^2/2\,\sigma^2}}{\sqrt{2\pi}\sigma} \tag{7}$$

and

$$f(y) = \frac{1}{\pi\sqrt{a(z)^2-(y-1)^2}} \tag{8}$$

Substituting Eqs. (7) and (8) in Eq. (6) results in

$$h(I) = h_0 \int_{u_{min}}^{u_{max}} du\, \frac{e^{-u^2}}{\sqrt{(u_{max}-u)(u-u_{min})}} \tag{9}$$

where

$$h_0 = \frac{1}{\sqrt{2\pi^3}\sigma\sqrt{1-a(z)^2}} \tag{10}$$

is the normalization constant and

$$u_{max} = \frac{I-(1-a(z))}{\sqrt{2}\sigma(1-a(z))} \tag{11}$$

$$u_{min} = \frac{I-(1+a(z))}{\sqrt{2}\sigma(1+a(z))} \tag{12}$$

are the integration limits. Although expression (9) does not have a closed analytical solution, it can be numerically integrated.

Fig. 4 shows the pdfs $g(x)$ and $f(y)$, for both random variables, x and y, respectively, and $h(I)$ associated to $I(z)$, resulting from Eq. (9) assuming a contrast parameter $a(z)=1$. It is worthy to note that the variation range of $f(y)$, and thus of $h(I)$, given by the Eqs. (11) and (12), strongly depends on the contrast parameter value. If the $a(z)$ value is close to 1 ($z \ll Cl$) the intensity distribution will be similar to that of Fig. 4, with the extreme values close to 0 and 2. As the optical path difference increases and the $a(z)$ value approaches 0 ($z \gg Cl$), the $h(I)$ pdf will resemble the Gaussian pdf centered in 1. Finally, although the 1000 data acquired for each z value define a mean value and a standard deviation with great precision, well resolved histograms are required to evaluate Eq. (9) and, in consequence, to determine $a(z)$. As the *bin* size is reduced, the histogram becomes noisier and the experimental data were therefore fitted with the cumulative distribution function (cdf, Eq. 13) with σ and $a(z)$ as the only fitting parameters.

$$H(I) = \int_0^I ds\ h(s) \tag{13}$$

4. Results and discussion

Thirteen series of 1000 data associated to each of the 13 positions of mirror M4, and thus to the optical path difference z, were obtained. Fig. 5 shows the histograms obtained for three values of the optical path difference. It can be noted that for z about 1 m the pdf is essentially Gaussian while in the other two cases, z close to cero and about 2.5 m, it resembles the pdf $h(I)$ shown in Fig. 4. These results indicate that $a(z)$ is close to one in the extreme cases and close to zero in the intermediate case.

As mentioned in the previous section, although the histograms associated to the pdf $h(I)$ are clearer and more intuitive, the data were analyzed using the cdf given by Eq. (13).

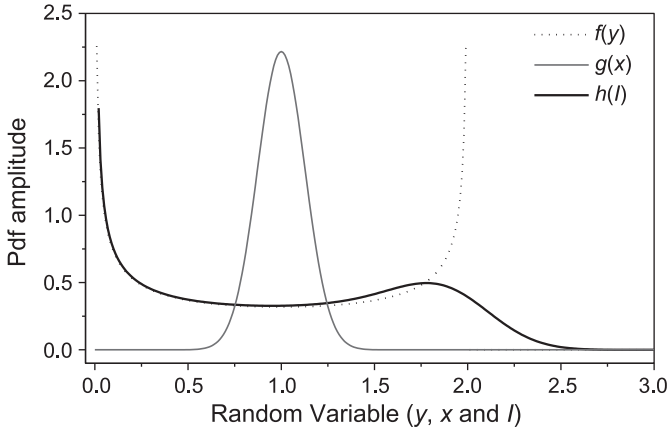

Fig. 4. Pdfs $g(x)$, $f(y)$ and $h(I)$ associated to the two random variables, x and y, and to their product, I.

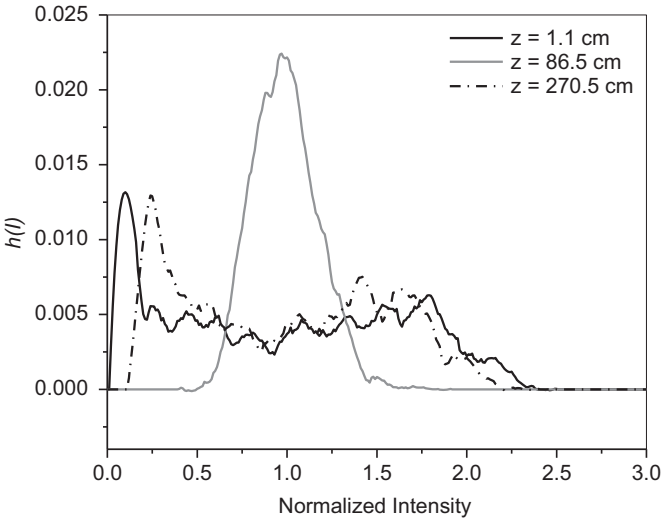

Fig. 5. Experimental histograms $h(I)$ obtained for three values of z.

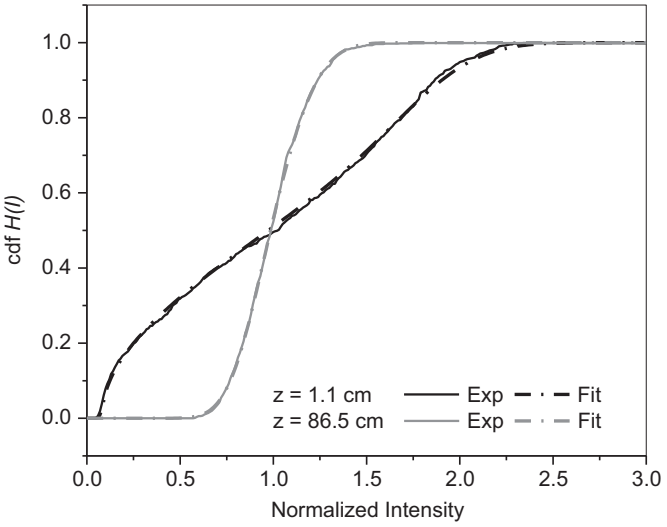

Fig. 6. Experimental (Exp) and calculated (FIT) cumulative distribution functions H(I) for two optical path differences.

Fig. 6 shows the excellent correlation obtained between experimental and calculated cdf $H(I)$ for two z values in two extreme $a(z)$ conditions. The contrast parameter values $a(z)$ for the 13 z values were determined in the same manner and the results are shown in Fig. 7. Qualitative results shown in Fig. 5 can be quantitatively appreciated: the contrast parameter decreases with increasing optical path difference to about 1 m and then increases reaching a 2nd maximum for $z=271$ cm. This second maximum at $z=2L$ corresponds to mode beating. A coherence length, $Cl=40$ cm, was estimated from the value of $a(z)$ for which the contrast parameter falls to 0.5.

Eq. (3) was used to calculate the values of $a(z)$ with the total number of longitudinal modes, N, the amplitudes of each mode, b_n, and the coherence length of each individual mode, γ^{-1}, as the fitting parameters. The fitting criterion used is as follows. First, in order to reduce the number of parameters of the model, the oscillating modes were assumed to be symmetrical about the center of the curve gain, i.e. $b_n=b_{-n}$, and therefore, for n varying between 1 and N, $2N+1$ modes oscillated. Then, the N value was obtained as the smallest value for which the fitting mean square error did not vary significantly. The values resulting from the fit are summarized in Table 1. $N=3$ indicates that, in the average,

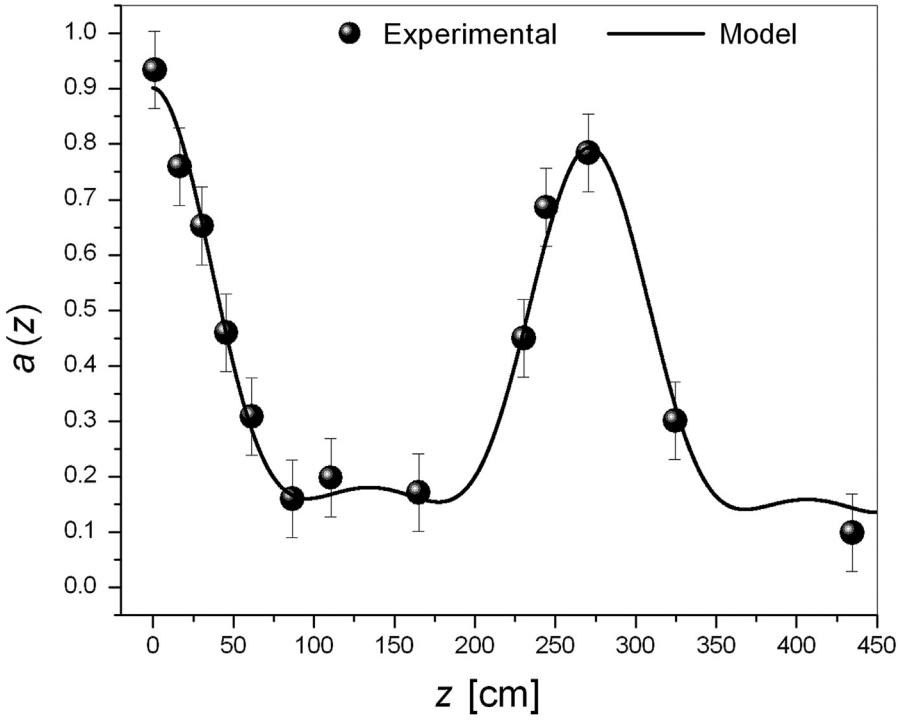

Fig. 7. Contrast parameter variation with the optical path difference obtained from the fitting. Symbols: experimental values; solid line: calculated values.

Table 1
Parameters obtained with the model.

N	3
b_1	0.463 ± 0.039
b_2	0.186 ± 0.037
b_3	0.046 ± 0.031
γ^{-1}	14.2 ± 3.3 m

7 modes with amplitudes between b_1 and b_3 normalized to $b_0=1$ oscillated. The resultant coherence length of each individual mode was 14 m. This value is consistent with that estimated from $\gamma^{-1}=c\tau_p$, where c is the light speed and τ_p the pulse duration, for a pulse of about 60 ns. As it can be seen in Fig. 7 an excellent agreement between experimental and calculated values was obtained.

Finally, a spectral analysis of the time series detected at the interferometer input was performed and the results were compared with those of the interferometric method. A typical bandwidth limited pulse (20 MHz) acquired to obtain a well defined peak value, the observable of interest, was shown in Fig. 2. The time profile of the pulse obtained with detector D1 with a 1 GHz bandwidth in which the longitudinal mode beating can be observed is shown in Fig. 8.

Assuming, as it was mentioned before, that the pulse can be described by a superposition of the different modes with wave numbers $k_n=k_0+n\pi/L$ and normalized amplitudes b_n, the Fourier transform of the pulse will be a train of peaks centered in the frequencies determined by modes' frequencies subtraction:

$$f_n = n\frac{c}{2L} \tag{14}$$

with amplitudes:

$$J(f_n) = J(0)\begin{cases} 1 & n=0 \\ \frac{1}{2}\sum_{m=-N}^{N-n}\sqrt{b_m b_{m+n}} & 1\le n\le 2N \end{cases} \tag{15}$$

From the Fast Fourier Transform, FFT, of 1000 time series like that shown in Fig. 8, 1000 frequency spectra were obtained. Fig. 9 shows the average spectral power density of the 1000 frequency spectra. Since the cavity length was $L=135$ cm, the frequencies are multiples of 110 MHz (Eq. 15). A coherence length of about 40 cm with a 7 modes beat and a single mode coherence of 14.2 m (γ^{-1}) were obtained with the interferometric method. This is associated in the Fourier spectrum to a total bandwidth of 750 MHz and a peak width of about 20 MHz, in very good agreement with the spectral power density shown in Fig. 9. The values calculated with expression 14 are presented as well in the figure. The points were connected with lines only to guide the eye. It is worthy to outstand that the only fitting parameter of the curve predicted by the model is a scale factor that links the spectral power density to the photon density. The appearance of a peak at 770 MHz with an amplitude about 1000 times lower than the maximum of the gain curve is due to the sporadic oscillation of an eighth mode very close to the lasing threshold.

5. Conclusions

A Michelson interferometer of about 5 m of optical path length difference was built with a motorized translation optical mount in one arm. Transversal monomode and longitudinal multimode lasing was attained by filtering the higher spatial frequencies with an intracavity iris. A stochastic method for data acquisition and analysis was developed. This method is robust enough and does not require the usual high stability of the table and optics of the interferometric experiments. However, in order to perform good statistics, it requires large amounts of data which is not a problem with an automated acquisition system.

A coherence length of 40 cm was determined for our TEA CO_2 laser. Moreover, it could be proved that the laser coherence is given by the longitudinal mode beating modulated by the individual spatial coherence of each mode. The oscillation of 7 longitudinal modes and a laser bandwidth of about 700 MHz could be determined from the comparison of the experimental contrast parameter with that calculated with the model. At the same time, the relative weight and the coherence length of each of those modes was determined. The value of 14 m of this last parameter is in good agreement with the spatial pulse width.

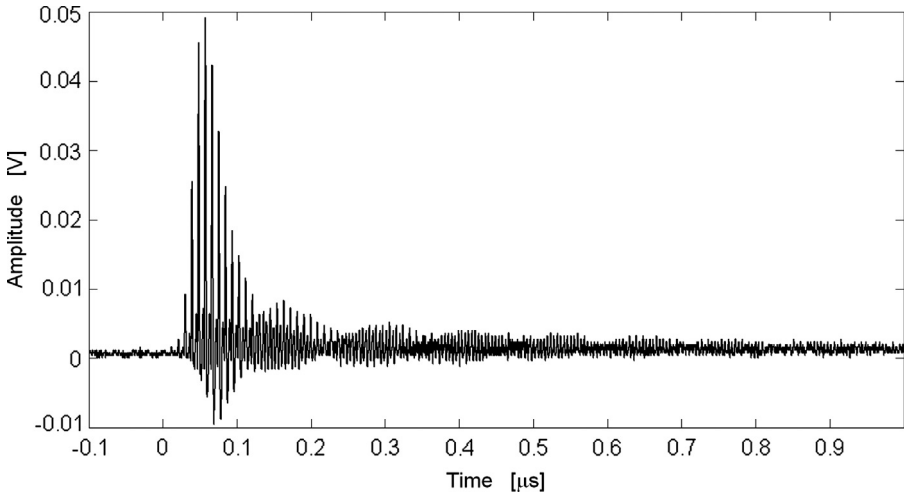

Fig. 8. Typical time series obtained with the photon drag detector, D1, for transverse monomode (TEM_{00}) and longitudinal multimode lasing.

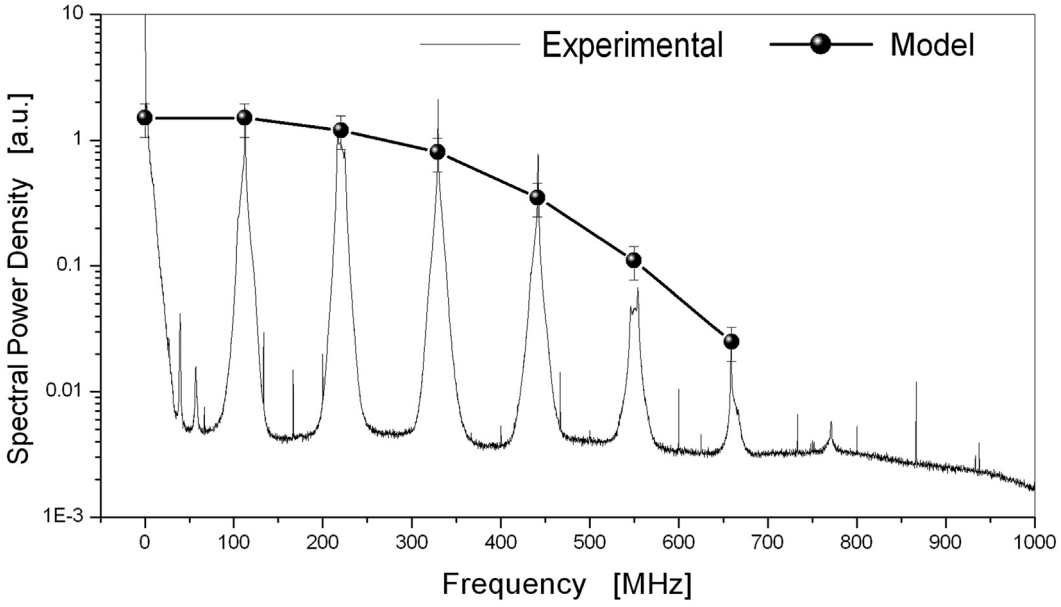

Fig. 9. Spectral power density of the longitudinal multimode pulse of Fig. 8.

Finally, the results were compared with those obtained with a spectral method. Global and individual mode coherence lengths values in good agreement with those attained with the interferometric method were achieved from the frequency spectrum of the pulse.

Although similar values of the laser bandwidth and of the global and single mode coherence lengths are obtained with both methods, it must be emphasized that the stochastic method developed in this work gives a larger amount of information in a more precise manner.

Acknowledgment

This research has been supported by the grant PIDDEF no. 009/11 from the Ministerio de Defensa of Argentina.

References

[1] Cantrell CD. Multiple-photon excitation and dissociation of polyatomic molecules. Berlin, Heidelberg, New York: Springer; 1986.

[2] Letokhov VS. Nonlinear laser chemistry. Berlin, Heidelberg, New York: Springer; 1983.

[3] Bagratashvili VN, Letokhov S, Makarov AA, Ryabov EA. Multiple photon infrared laser photophysics and photochemistry. London, Paris, New York: Harwood, Chur; 1985.

[4] Freytes VM, Codnia J, Azcárate ML. Intracavity system design for IR multiphoton dissociation. Applied Physics B 2011;103:687–93.

[5] Vazquez MA, Azcárate ML, Quel EJ, Doyennette L, Rinaldi C, Ferrero JC. Vibrational relaxation of the $2\nu_5$ overtone of $CDCl_3$ following TEA CO_2 laser excitation of the ν_4 mode. Laser Chemistry 1994;14:19–200.

[6] Vazquez MA, Azcárate ML, Quel EJ, Doyennette L, Rinaldi C, Ferrero JC. Vibrational relaxation of the $2\nu_5$ overtone of $CDCl_3$ highly excited by a TEA CO_2 laser. Laser Chemistry 1994;15:61–9.

[7] Alcaraz AN, Codnia J, Azcárate ML. Infrared Multiphoton dissociation of SiF_4: gas phase reactions of SiF_3 with F and H_2. Journal of Photochemistry and Photobiology A: Chemistry, 165; 209–14.

[8] Codnia J, Azcárate ML. Rate measurement of the reaction of CF_2Cl radicals with O_2. Photochemistry and Photobiology 2006;82:755–62.

[9] Alcaraz AN, Codnia J, Azcárate ML, SiF_4 IR. Photodissociation: gas phase reactions of SiF_3 with CH_4. Journal of Photochemistry and Photobiology A: Chemistry, 205; 79–83.

[10] Gómez ND, D'Accurso V, Codnia J, Manzano FA, Azcárate ML. Direct determination of the dissociation probability in highly focused IR multiple photon dissociation. Applied Physics B 2012;106:921–6.

[11] Makowe J, Boyarkin OV, Rizzo TR. Isotopically selective infrared multiphoton dissociation of vibrationally excited SiH_4. Journal of Physical Chemistry A 2002;106:5221–9.

[12] Yokoyama A, Ohba H, Hashimoto M, Katsumata K, Akagi H, Ishii T, et al. Silicon isotope separation utilizing infrared multiphoton dissociation of Si_2F_6 irradiated with two-frequency CO_2 laser lights. Applied Physics B 2004;79:883–9.
[13] Polianski M, Boyarkin OV, Rizzo TR, Apatin VM, Laptev VB, Ryabov EA. Infrared laser chemistry of trichlorosilane in view of silicon isotope separation. Journal of Physical Chemistry A 2003;107:8578–83.
[14] Siegman AE. Lasers. Mill Valley, California: University Science Books; 1986.
[15] Mathieu P, Izat JR. Narrow-band CO_2 TEA laser for efficient FIR laser pumping. IEEE Journal of Quantum Electron, QE 1977;13:465–8.
[16] Gatenby PV, Hawkins KC, Rutt HN. Line narrowed TEA CO2 laser for optical pumping of molecular gas lasers. Journal of Physics E Scientific Instruments 1981;14:56–7.
[17] Yu Baranov V, Baronov GS, Dyad'kin AP, Kazakov SA, Kolesnikov Yu a, Kotov aA, et al. Optically pumped pulse-periodic CF_4 laser. Quantum Electronics 1996;26:762–4.
[18] Chin SL. Various techniques for producing a single longitudinal mode TEA-CO_2 laser. Optics and Laser Technology 1980:85–8.
[19] Dougal RA, Gundersen MA, Williams PF. Simple powerful tunable single-mode and mode-locked TEA CO_2 laser. Review of Scientific Instruments 1982;53:181–3.
[20] Gordienko VM, Putivskii YuYa. Spectral characteristics of a TEA CO_2 laser with external signal injection. Soviet Journal of Quantum Electronics 1991;21:284–6.
[21] Duarte FJ. Variable linewidth high-power TEA CO_2 laser. Applied Optics 1985;24:34–7.
[22] Kunets AV, Kuritsyn YuA, Makarov GN, Mironenko VR, Pak I. Diode laser measurements of a pulsed TEA CO_2 laser linewidth. Optics Communications 1991;84:37–41.
[23] Demtröder W. Laser spectroscopy. Berlin, Heidelberg, New York: Springer; 1998.